Fermi-liquid-to-polaron crossover. II. Double exchange and the physics of colossal magnetoresistance

A. J. Millis, R. Mueller, and Boris I. Shraiman

Bell Laboratories, Lucent Technologies, 600 Mountain Avenue, Murray Hill, New Jersey 07974

We use the dynamical mean-field method to study a model of electrons Jahn-Teller coupled to localized classical oscillators and ferromagnetically coupled to "core spins." The model, we argue, contains the essential physics of the "colossal magnetoresistance" manganites $Re_{1-x}A_xMnO_3$. We determine the different regimes of the model and present results for the temperature and frequency dependence of the conductivity, the electron spectral function, and the root-mean-square lattice parameter fluctuations. We compare our results to data and give a qualitative discussion of important physics not included in the calculation. Extensive use is made of results from a companion paper [Phys. Rev. B **54**, 5389 (1996)]. [S0163-1829(96)09431-3]

I. INTRODUCTION

The doped rare-earth manganites have been studied for many years[1,2] and interest in the materials has revived following the recent discovery of extremely large magnetoresistance in some members of the family.[3] The chemical formula is $Re_{1-x}A_xMnO_3$, with Re a rare-earth element such as La or Nd and A a divalent metal ion such as Sr or Ca. The electronically active orbitals are believed to be the Mn d orbitals[1,2] and the mean d occupancy is $4-x$. Each Mn ion feels an approximately cubic crystal field, which splits the Mn d levels into a t_{2g} triplet and an e_g doublet.[4] The t_{2g} levels are believed[2,5] to lie substantially (~ 5 eV) below the e_g levels. On-site Coulomb interactions are apparently strong enough that no d orbital may be occupied by more than one electron. Further, all electron spins in Mn d orbitals are aligned by a large ferromagnetic Hunds rule coupling. The Coulomb and Hunds rule interaction energies have not been measured directly, but there is substantial indirect evidence that they are large. For example, at $0.2 \lesssim x \lesssim 0.5$ (precise values depend on Re and A) the ground state is ferromagnetic, and the observed magnetization is consistent with all $4-x$ electrons on each Mn being lined up in the maximal spin state,[1] suggesting a large Hunds coupling. Also, $ReMnO_3$ undergoes a structural phase transition at $T \approx 800$ K, which has been shown[6,7] to be due to a staggered (π, π, π) ordering of Jahn-Teller distortion of local e_g symmetry. This would not occur unless the e_g orbital were singly occupied, which in turn implies that the t_{2g} orbitals are also singly occupied, suggesting a large on-site Coulomb interaction.

The resulting physical picture is that 3 of the $(4-x)$ d electrons fill up the t_{2g} levels, forming an electrically inert core spin $\vec{S}_c$ of magnitude $S_c = 3/2$. The remaining $1-x$ electron goes into a linear combination of the e_g levels, and is coupled to $\vec{S}_c$ by a Hunds rule coupling J_H, which is presumably large, but has not been directly measured. Okimoto *et al.* have recently presented an interpretation of optical data implying that $J_H S_c \sim 1.2$ eV.[8] We shall argue below that their interpretation is not correct and that $J_H S_c$ is rather larger. Certainly, the conventional[1] wisdom is that the limit $J_H S_c \to \infty$ is appropriate, so one only need consider configu-

rations with e_g electrons parallel to core spins.

The $Re_{1-x}A_xMnO_3$ materials display a wide range of interesting physics. For $0 \leq x \lesssim 0.2$ (all x values are approximate, and depend on Re and A) the materials are insulating at all temperatures and are antiferromagnetic or ferrimagnetic at low T. For $0.2 \lesssim x \lesssim 0.5$ the low-T phase is a fully polarized ferromagnetic metal. As the temperature is increased for $0.2 \lesssim x \lesssim 0.5$, there is a ferromagnet-to-paramagnet transition, which may be of first or second order, at a $T_c(x) \sim 300$ K. In the paramagnetic state the material may be either "metallic" (in the sense that $d\rho/dT > 0$ and $\rho \lesssim \rho_{Mott}$) or "insulating" (in the sense that $d\rho/dT < 0$ and $\rho \gtrsim \rho_{Mott}$). [Here ρ_{Mott}, the Mott "maximum metallic resistivity," is about ~ 1000 $\mu\Omega$ cm and corresponds to a mean free path of order p_F^{-1} (Ref. 9).] Insulating behavior occurs at lower x and metallic behavior at higher x. There is for all x a very pronounced drop in ρ as T is lowered through T_c, and in this regime the resistivity has a very strong magnetic field dependence. The "colossal" magnetoresistance of interest here occurs for x such that the material is in the "insulating" regime at $T > T_c$ but is a metallic ferromagnet at $T < T_c$. Finally, at $x \gtrsim 0.5$ the low-T state is charge ordered, antiferromagnetic, and insulating.[1,10] We do not address the physics of this regime here. A qualitative phase diagram is shown in Fig. 1.

Most models[11–15] of electron transport in $Re_{1-x}A_xMnO_3$ have emphasized the "double exchange" phenomena caused by the large Hunds coupling J_H. The essence of double exchange is that when an electron hops from site i to site j it must also go from having its spin parallel to $\vec{S}_c^i$ to having its spin parallel to $\vec{S}_c^j$; the hopping amplitude t_{ij} thus depends upon relative spin orientation.[11] For two fixed sites i and j it is possible to choose phase factors so that $t_{ij} \to (t_{ij}/\sqrt{2})\sqrt{1 + \vec{S}_c^i \cdot \vec{S}_c^j / S_c^2} \equiv t_{ij}\cos[\theta_{ij}/2]$.

The double exchange phenomenon gives an obvious connection between electron hopping and magnetic order: disorder in the spins implies randomness in t_{ij}, which decreases below T_c or in a field. This effect seems very likely to be related to the "colossal" magnetoresistance observed near T_c. However, two of us and Littlewood have recently argued
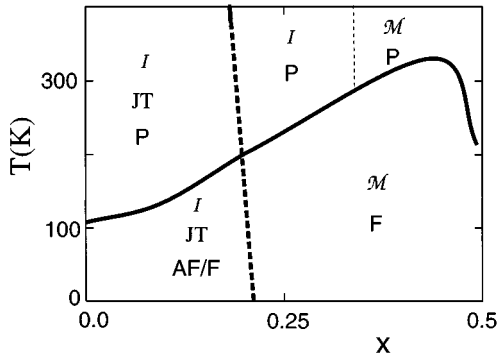
FIG. 1. Qualitative temperature- (T-) doping (x) phase digram of $Re_{1-x}A_xMnO_3$, with magnetic phases (F, ferromagnet; AF, antiferromagnet; P, paramagnet), structural phases (JT, Jahn-Teller order; no label, no order), and transport regimes (M, ''metal,'' $d\rho/dT>0$; I, ''insulator,'' $d\rho/dT<0$) indicated. The solid lines are magnetic phase boundaries, the heavy dashed line is the Jahn-Teller boundary, and the light dotted line is the metal-insulator crossover. For $x>0.5$ different physics, involving charge ordering, is important at low T. Different materials may have phase diagrams differing in some details, and the magnetic and structural boundaries may not coincide at low T.

that models involving only double exchange cannot explain the observed resistivity.[16] The essential point is that in materials exhibiting ''colossal'' magnetoresistance the resistivity at $T>T_c$ is much larger than the Mott limit and moreover rapidly increases as T decreases. Indeed, as shown in Appendix A, the observed $T>T_c$ resistivities are so large that a classical description involving particles incoherently hopping from site to site with a hopping probability $W \ll k_B T/\hbar$ is appropriate. In models involving only double exchange the scattering produced by spin disorder is simply not large enough to cause such insulating behavior. A straightforward calculation[14,16] shows that if the spins are completely decorrelated one finds $p_F \ell \sim 3$, i.e., $W \sim t_{ij} \gg kT$. More sophisticated arguments involving localization and phase factors are shown in Appendix B not to change this conclusion significantly. Therefore we believe some additional physics not included in the double exchange-only model must be important. This conclusion is not universally accepted.[15,17]

One possible source of this extra physics is the ''Hubbard U'' effect of the on-site Coulomb interaction, which produced the Hunds coupling in the first place. While this is undoubtedly quantitatively important, we do not believe it is the primary cause of the observed insulating behavior, essentially because away from commensurate densities (such as one electron per site) canonical Mott insulating materials such as the high-T_c superconductors or other doped transition-metal oxides have resistivities that are rather less than the Mott limit and that decrease with temperature,[18,19] in stark contrast to the behavior observed at $T>T_c$ in $Re_{1-x}A_xMnO_3$.

We proposed[16] that the crucial additional physics is a strong electron-phonon coupling, which localizes the conduction electrons as polarons at $T>T_c$ and smaller x, but is weakened in the $T<T_c$ ferromagnetic state, restoring metallic behavior. We argued that this is possible because the behavior of the electron-phonon model is controlled by a

dimensionless coupling parameter, which is the ratio of an interaction energy to the electron kinetic energy. The double exchange physics implies that ferromagnetic order increases the electron kinetic energy, thereby decreasing the effective coupling strength. Also, a recent analysis[20] of the structural distortion observed[7] in $LaMnO_3$ showed that the electron-phonon coupling is indeed strong.

In this paper we present a detailed study of a model of electrons coupled to core spins and to phonons, which we believe confirms the importance of electron-phonon interactions. We use a ''dynamical mean-field'' method, which has previously been extensively applied to interacting problems without double exchange[21] and has been used by Furukawa to study models involving only double exchange.[15] The model we study does not capture all of the physics of $Re_{1-x}A_xMnO_3$; in particular, Coulomb effects and quantum and intersite terms in the phonon Hamiltonian are omitted and an oversimplified electron-phonon coupling is used. We therefore cannot quantitatively compare our results to experiment. The qualitative agreement we obtain is, however, compelling.

Other workers have also studied electron-phonon effects in manganites and related materials. Emin, Hillery, and Liu studied a theoretical model of a single bound polaron coupled to spin waves and found a temperature dependence of the polaron size that they argued could be related to transport anomalies at T_c observed in EuO.[22] Their work involves only a single electron and is based on a model in which double exchange is not relevant, reflecting the different physics of EuO. Roder, Zang, and Bishop used variational wave function techniques to examine the interplay between electron-phonon interaction and double exchange.[23] Their work is in a sense complementary to ours. They have incorporated quantum phonons and have presented some results on intersite phonon correlations, but their technique seems to work best at low temperatures. To calculate properties at and above T_c they resort to a dilute limit approximation, which amounts to the study of a single carrier in a deformable medium. Also, they have not presented results for transport and optical quantities; their main result is a calculation of the coupling dependence and doping dependence of T_c. Their results for the coupling dependence are very similar to ours; their results for the doping dependence are based on an assumption that, we argue, is not justified by the arguments in their paper. A comparison of their results for T_c to ours is given in Sec. IV, and a further discussion is given in the Conclusion.

The rest of this paper is organized as follows. In Sec. II we define the model and the approximations used. In Sec. III we give the qualitative physics of the model, distinguishing different regimes and presenting the behavior of physical quantities in each. In Sec. IV we present the results of a detailed numerical study of the model at half filling. In Sec. V we present and discuss results at other dopings. Section VI is a conclusion, in which the relation of results to data is analyzed and the effects of omitted interactions are outlined. Appendix A discusses the theoretical interpretation of the observed resistivities, in particular the relation to the Mott minimum metallic conductivity and to transport by classical particles, while Appendix B discusses in more detail the resistivity of the double-exchange-only model. An announce-

ment of some of the results of this paper will appear elsewhere.[24]

This paper relies heavily on results of a companion paper, which uses the dynamical mean-field method to study electron-phonon interactions in models without double exchange,[25] to which we refer henceforth as I.

II. MODEL AND APPROXIMATIONS

We study a model of Mn e_g d electrons coupled to core spins $\vec{S}_c^i$ and phonons, with Hamiltonian

$$H = H_{\text{band}} + H_{d\text{-ex}} + H_{\text{el-ph}} + H_{\text{ph}}. \tag{1}$$

H_{band} describes the hopping of d electrons between sites i,j of a lattice. We take the electrons to have twofold orbital degeneracy labeled by a roman index (a,b) and twofold spin degeneracy labeled by a greek index (α, β). Explicitly,

$$H_{\text{band}} = -\sum_{\langle ij \rangle ab\alpha} t_{ij}^{ab} d_{ia\alpha}^\dagger d_{jb\alpha} - \mu \sum_{ia\alpha} d_{ia\alpha}^\dagger d_{ia\alpha}. \tag{2}$$

The hopping matrix element t_{ij}^{ab} is a real symmetric matrix whose form depends on the choice of basis in ab space and the direction of the i-j bond. The precise form will not be important in what follows.

The interaction of itinerant electrons with the core spins is given by

$$H_{d\text{-ex}} = -J_H \sum_{ia\alpha\beta} \vec{S}_c^i \cdot d_{ia\alpha}^\dagger \vec{\sigma}_{\alpha\beta} d_{ia\beta}. \tag{3}$$

As discussed below, we shall take the limit $J_H S_c \to \infty$.

We assume a Jahn-Teller form for the electron-phonon coupling. Previous analysis[6,20] has shown that this coupling is strong in $LaMnO_3$, so it may be expected to be strong also in doped compounds. Thus we focus on lattice distortions that split the on-site orbital degeneracy of the e_g levels. Physically, these correspond to e_g symmetry distortions of the oxygen octahedra around a Mn site. Mathematically, we may parametrize a local e_g distortion by a magnitude r and an angle θ, and define a two-component vector $\vec{r} = (r_z, r_x)$ with $r_z = r\cos\phi$ and $r_x = r\sin\phi$. The coupling of this to the e_g levels is prescribed by group theory[4] to be

$$H_{\text{el-ph}} = g \sum_{iab\alpha} \vec{r}_i \cdot d_{ia\alpha}^\dagger \vec{\tau}_{ab} d_{ib\alpha}. \tag{4}$$

Here $\vec{\tau} = (\tau^z, \tau^x)$ is a vector of Pauli matrices acting in orbital space.

It is important to note that the coupling written in Eq. (4) is not the only physically relevant one. In Ref. 20 it was argued that a Mn site with no e_g electrons would induce a breathing distortion of the surrounding oxygen ions, and that this breathing distortion played an important role in determining the x dependence of the structural phase boundary. We have not included this coupling in the present calculations, but will qualitatively discuss its effects in the Conclusion.

In order to obtain a tractable model we assume H_{ph} describes classical harmonic oscillators of stiffness k, which are furthermore independent from site to site. Thus,

$$H_{\text{ph}} = \sum_i \frac{1}{2} k r_i^2. \tag{5}$$

Despite the simplifying approximations, the model defined by Eq. (1) is not solvable except in certain limits. To obtain results, we adopt the ''dynamical mean-field'' approximation, which becomes formally exact in a limit in which the spatial dimensionality $d \to \infty$ and has been shown to provide a reasonable description of models of interacting electrons in $d = 3$.[21] Recently, the technique has also been applied to the double-exchange-only model defined by Eq. (1) with $H_{\text{el-ph}} = 0$.[15] The resulting resistivity is very similar to that obtained using other techniques,[14] further confirming the accuracy of the method.

The dynamical mean-field method is based on an assumption about the electron Green function $G_{\alpha\beta}^{ab}(p, \omega)$. In general this is a tensor in spin and orbital space, which may be written as

$$[G_{\alpha\beta}^{ab}(p, \omega)]^{-1} = \omega - \epsilon_p^{ab} + \mu - \Sigma_{\alpha\beta}^{ab}(p, \omega) \tag{6}$$

Here ϵ_p^{ab} is the dispersion implied by Eq. (2) and Σ is the self-energy due in the present problem to $H_{\text{el-ph}}$ and $H_{d\text{-ex}}$. The fundamental approximation of the dynamical mean-field method is the neglect of the momentum (p) dependence of Σ. This is a reasonable approximation because models of the form of Eq. (1) (such as the usual Migdal-Eliashberg electron-phonon Hamiltonian) generally lead to a self-energy with a weak momentum dependence in $d = 3$.[26] If the momentum dependence of Σ may be neglected, then all physical quantities may be expressed as functionals of the momentum-integrated Green function G_{loc}, given by

$$G_{\text{loc}\alpha\beta}^{ab}(\omega) = \int \frac{d^3p}{(2\pi)^3} G_{\alpha\beta}^{ab}(p, \omega). \tag{7}$$

We shall assume that there is no long-range order in orbital space, so G_{loc} and also $\Sigma(\omega)$ must be proportional to the unit matrix in ab space. We shall allow for the possibility of ferromagnetic order, and shall take the ordered moment parallel to $\mathbf{z}$. We may then write

$$G_{\text{loc}\alpha\beta}^{ab}(\omega) = g_0(\omega) + g_1(\omega)\sigma^z \tag{8}$$

and a similar equation for Σ. We simplify Eq. (7) by first writing $g_{0,1} = 1/4 \text{Tr}_{ab}\text{Tr}_{\alpha\beta} \int d^3p/(2\pi)^3 G_{\alpha\gamma}^{ab}(\sigma_{\gamma\beta}^z)^{0,1}$, then introducing at each p the rotation matrix R_p^{ab}, which diagonalizes ϵ_p^{ab} i.e.,

$$\epsilon_p^{ab} = R_p \begin{bmatrix} \epsilon_p^1 & 0 \\ 0 & \epsilon_p^2 \end{bmatrix} R_p^{-1} \tag{9}$$

and finally exploiting the cyclic invariance of the trace. We obtain

$$g_0(\omega) = \frac{1}{4} \text{Tr}_{ab}\text{Tr}_{\alpha\beta} \int d\epsilon_p \mathcal{D}(\epsilon_p)[\omega - \epsilon_p + \mu - \Sigma_{\alpha\beta}(\omega)]^{-1},$$

$$\tag{10}$$

$$g_1(\omega) = \frac{1}{4}\mathrm{Tr}_{ab}\mathrm{Tr}_{\alpha\beta}\int d\epsilon_p \mathcal{D}(\epsilon_p)\sigma^z$$

$$\times[\omega - \epsilon_p + \mu - \Sigma_{\alpha\beta}(\omega)]^{-1},$$

where ϵ_p is either of the eigenvalues of ϵ_p^{ab} (they are related by symmetry operations) and $\mathcal{D}$ is the density of states, which we take to be semicircular with width $D = 4t$:

$$\mathcal{D}(\epsilon_p) = \sqrt{4t^2 - \epsilon_p^2}/2\pi t^2. \tag{11}$$

Because G_{loc} is momentum independent and involves two independent functions, it must be the Green function of some effective single site model involving two mean-field functions a_0 and a_1. This model is described by the partition function

$$Z_{\mathrm{loc}} = \int r\,dr\,d\phi \int d^2\vec{\Omega}_c \exp[S_{\mathrm{loc}}]. \tag{12}$$

Here r and ϕ are the classical oscillator coordinates introduced above Eq. (4), $\vec{\Omega}_c = \vec{S}_c/|S_c|$, and the integrals are simple integrals rather than functional integrals because we have taken r, ϕ, and $\vec{\Omega}_c$ to be classical.

The effective action S_{loc} is

$$S_{\mathrm{loc}} = -\frac{1}{2}\frac{k}{T}r^2 + \sum_n \mathrm{Tr}\ln[a_0(i\omega_n) + a_1(i\omega_n)\sigma_z$$

$$+ J_H\vec{\Omega}_c\cdot\vec{\sigma}_{\alpha\beta} + g\vec{r}\cdot\vec{\tau}_{ab}] - \vec{h}_{\mathrm{ext}}\cdot S_c\vec{\Omega}_c/T. \tag{13}$$

Here we have added a term coupling the core spin to an external field $\vec{h}_{\mathrm{ext}}$. One could also couple the external field to the e_g electrons, but the factor of $3/(1-x)$ in size of moment means that this coupling is unimportant.

The mean-field parameters a_0, a_1 in Eq. (13) are determined as follows.[21] One obtains the local Green functions $g_{0,1}^{\mathrm{loc}} = 1/4\,\delta\ln[Z_{\mathrm{loc}}]/\delta a_{0,1}$, defines from these self-energies $\Sigma_{0,1} = a_{0,1} - (g_{0,1}^{\mathrm{loc}})^{-1}$, and demands that $\Sigma_{\alpha\beta} \equiv \Sigma_0 + \Sigma_1\sigma_z$ reproduces $g_{0,1}^{\mathrm{loc}}$ when used in Eqs. (10) and (8). For the semicircular density of states the resulting equations may be written as

$$a_0(\omega) = \omega + \mu - \frac{t^2}{4}\frac{\delta\ln[Z_{\mathrm{loc}}]}{\delta a_0(\omega)},$$
$$\tag{14}$$

$$a_1(\omega) = -\frac{t^2}{4}\frac{\delta\ln[Z_{\mathrm{loc}}]}{\delta a_1(\omega)}.$$

The factor of four is that appearing in Eq. (10).

These equations simplify in the ''double exchange'' limit $J_HS_c \to \infty$. The argument of the Tr ln in Eq. (13) is a matrix in the direct product of spin and orbital space. It has four eigenvalues, $a_0 \pm \Delta \pm gr$ with $\Delta = |a_1\hat{z} + J_HS_c\vec{\Omega}|$. These are, of course, independent of the angle ϕ describing the phonon. For $J_HS_c \gg t$ the eigenvalues at $a_0 - \Delta \pm gr$ correspond to high-energy states that do not affect low-energy phenomena. Further, from Eq. (14) it is clear that a_1 is of order t, so $a_1 \ll J_HS_c$ and we may approximate $\Delta \approx J_HS_c + a_1\Omega_z$. We

may then absorb the constant term J_HS_c into a_0 and μ, rescale the parameters, and define the spin angle θ via $\Omega_z = \cos(\theta)$ obtaining

$$S_{\mathrm{loc}}(x,\theta) = -\frac{x^2}{2T} + \sum_n \ln[(b_0 + b_1\cos\theta)^2 - \lambda x^2]$$

$$+ h_0\cos\theta/T. \tag{15}$$

Here $x = r\sqrt{k/t}$, $b_{0,1} = a_{0,1}/t$, $\lambda = g^2/kt$, $h_0 = h_{\mathrm{ext}}S_c/t$, and T, ω, and μ are measured in units of t. The mean-field equations become

$$b_0 = \omega + \mu - \frac{1}{2}\int_0^\infty x\,dx\int_{-1}^1 d(\cos\theta)P(x,\theta)$$

$$\times\frac{(b_0 + b_1\cos\theta)}{(b_0 + b_1\cos\theta)^2 - \lambda x^2},$$
$$\tag{16}$$

$$b_1 = -\frac{1}{2}\int_0^\infty x\,dx\int_{-1}^1 d(\cos\theta)P(x,\theta)\cos\theta$$

$$\times\frac{(b_0 + b_1\cos\theta)}{(b_0 + b_1\cos\theta)^2 - \lambda x^2},$$

with

$$P(x,\theta) = \frac{1}{Z_{\mathrm{loc}}}\exp[S_{\mathrm{loc}}(x,\theta)]. \tag{17}$$

These equations differ from those discussed in I by the presence of the angular integral and by the quantity b_1, which expresses the spin dependence of G. Expressions for physical quantities are also slightly different from those used in I because we must keep track of the spin dependence.

The momentum integrated Green function has components parallel ($\uparrow\uparrow$) and antiparallel ($\downarrow\downarrow$) to the magnetization. The off-diagonal ($\uparrow\downarrow$) components vanish. We have

$$G_{\mathrm{loc}}^{\uparrow\uparrow}(\omega) = \omega + \mu - b_0(\omega) - b_1(\omega), \tag{18}$$

$$G_{\mathrm{loc}}^{\downarrow\downarrow}(\omega) = \omega + \mu - b_0(\omega) + b_1(\omega). \tag{19}$$

We shall be interested in the spectral function

$$A(\omega) = -\mathrm{Tr}\,\mathrm{Im}\mathbf{G}_{\mathrm{loc}}(\omega + i\delta)/\pi. \tag{20}$$

The conductivity is given by

$$\sigma(i\Omega) = \frac{2}{i\Omega}\int d\epsilon_p \mathcal{D}(\epsilon_p)T\sum_{i\omega}\mathrm{Tr}[\mathbf{G}(p,i\omega)\mathbf{G}(p,i\omega + i\Omega)], \tag{21}$$

where the factor of 2 comes from the trace over orbitals. Here $\mathbf{G}$ is a diagonal matrix in spin space and we have set $e = t = 1$.

Another interesting quantity is the electron kinetic energy K defined by

$$K = \mathrm{Tr}_{ab}\mathrm{Tr}_{\alpha\beta}\int \frac{d^3p}{(2\pi)^d}\epsilon_p^{ab}\langle d_{pa\alpha}^\dagger d_{pb\beta}\rangle. \tag{22}$$

By use of the relation between the expectation value and the electron Green function, of Eq. (6) with momentum independent self-energy, and of the arguments leading from Eq. (7) to Eq. (10) and the mean-field equations, we obtain

$$K = 2T \sum_n \, [G_{\text{loc}}^{\uparrow\uparrow}(\omega_n)]^2 + \sum_n \, [G_{\text{loc}}^{\downarrow\downarrow}(\omega_n)]^2. \tag{23}$$

The magnetization m is given by

$$m = \int_0^\infty x \, dx \int_{-1}^1 d\cos\theta \cos\theta P(x,\theta). \tag{24}$$

In these units the $T=0$ value of $m=1$.

We shall also be interested in the mean square lattice distortion $\overline{x^2}$, given by

$$\overline{x^2} = \int_0^\infty x \, dx \int_{-1}^1 d(cos\theta) x^2 P(x,\theta). \tag{25}$$

We conclude this section by mentioning numerical methods. We use the procedures described in I, and handle the additional angular integral by a twenty-point Legendre formula. Computations are of course more time consuming because of the extra integral involved. We found it convenient first to locate the magnetic transition temperature T_c and then to perform calculations at $T>T_c$ using equations obtained by forcing $b_1=0$. Convergence difficulties arise for temperatures near T_c; these are presumably related to critical slowing down near the magnetic phase transition. We found that an accurate value for T_c was most conveniently obtained by computing several values of m in the range $0.15 \lesssim m \lesssim 0.3$ ($0.02 \lesssim m^2 \lesssim 0.1$) and finding T_c by fitting to $m^2(T) = \alpha(T_c - T)$ with α and T_c fit parameters.

In previous work[16,24] we had also used an alternative method (which we termed the *projection method*) based on the observation that by choice of an appropriate local spin reference frame one may map the model into one of spinless fermions moving in a lattice with a spatially varying hopping determined by the local spin orientations. We further argued that within mean-field theory one could approximate this hopping by $t(m) = \sqrt{(1+m^2)/2}$, thereby simplifying the problem to one of spinless fermions, with hopping $t(m)$ coupled to phonons. Finally we argued that one could construct a mean-field magnetic free energy by combining the m dependence of the free energy of the auxiliary problem with the entropic term from the conventional mean-field theory for Heisenberg spins. This procedure leads to a $T_c(\lambda)/T_c(0)$ almost identical to that shown in Fig. 2; however, the *projection method* T_c is lower than those shown in Fig. 2. For example, the projection method T_c at $\lambda=0$, $\mu=0$ is $0.1t$, much less than the $0.17t$ shown in Fig. 2. A numerical error originally led us to believe the T_c's of the two approaches coincided. The discrepancy may most easily be understood by expanding $F = -T \ln[Z_{\text{loc}}]$ to order a_{1n}^2 The result is a quadratic form $\delta F \sim \Sigma_{mn} a_{1n} \Lambda_{nm} a_{1m}$. For example, at $g=0$, $\Lambda_{mn} = \delta_{mn}[1 - 1/3(a_{0n})^2] + 2/3 a_{0n} a_{0m}$. T_c is the temperature at which Λ first has a zero eigenvalue. The projection method result corresponds to setting $\Lambda_{mn} = \delta_{mn}[1 - 1/3(a_{0n})^2]$ and $a_{1n} = \text{const}$; in other words it produces a lower T_c because it does not permit an optimal
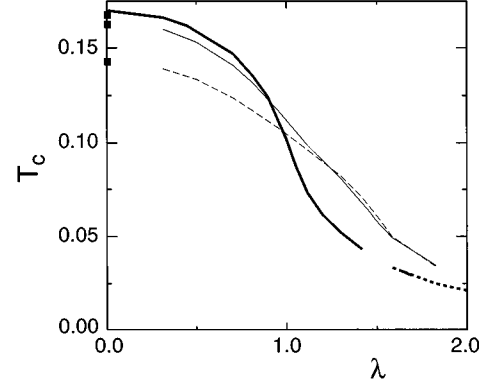

FIG. 2. Dependence of ferromagnetic T_c on coupling constant for $n=1$ (heavy solid line), $n=0.75$ (light solid line), and $n=0.5$ (light dashed line). The analytic zero coupling results are indicated by dots; the analytic strong coupling $T_c = n/12\lambda^2$ results by the heavy dotted line for $n=1$. Only for $n=1$ do the numerical calculations extend into the strong coupling regime.

choice of a_{1n}. We have therefore not used the projection method in this paper. We note, however, that the projection method provides a transparent and physically appealing motivation for the result, found also in the detailed calculations presented below, that the T_c is controlled by the kinetic energy at T_c.

III. QUALITATIVE BEHAVIOR

In this section we discuss the qualitative behavior of the solutions of Eqs. (16). Much of the behavior is similar to that found in I. The new feature is the physics of double exchange, which is expressed via b_1, via the angular integral and via the factors of $1/2$ on the right-hand side of Eqs. (16).

At $T \to 0$, the θ integral is dominated by the regime $\cos\theta=1$, so $b_1 = b_0 - (\omega + \mu)$. From Eq. (19) one sees that at $T=0$ the antialigned component of G vanishes, while the aligned component is determined by $(b_0 + b_1)$ which is given by an equation identical to that considered in I. Therefore, all of the results obtained in I for the $T \to 0$ limit hold also here. At $T>T_c$, there is no long-range magnetic order. Thus $b_1=0$, there is no θ dependence and b_0 is given by an equation that differs by a factor of $1/2$ from that treated in I.

Further insight into the quantity b_1 may be gained from the $\lambda=0$ limit. At $T=0$ and $\lambda=0$ the quantity $b_0 + b_1$ is found from Eqs. (14) to be

$$b_0 + b_1 = \frac{1}{2}[\omega + \mu - i\sqrt{4 - (\omega+\mu)^2}]. \tag{26}$$

This is precisely the usual noninteracting solution: $\text{Im}G_{\text{loc}} \neq 0$ in a semicircular band of full width $4t$. In the present conventions, the Fermi level is at $\omega=0$ and for $\lambda=0$ the maximum of the spectral function is at $\omega=-\mu$. The self-energy for this solution vanishes.

At $T>T_c$ and $\lambda=0$, $b_1=0$, and

$$b_0 = \frac{1}{2}[\omega + \mu - i\sqrt{2 - (\omega+\mu)^2}]. \tag{27}$$

Here $\text{ImG}_{\text{loc}} \neq 0$ in a semicircular band of full width $2\sqrt{2}t$: the fact that neighboring spins are uncorrelated has reduced the bandwidth, and thus the kinetic energy, by a factor of $\sqrt{2}$. This may also be seen by a direct evaluation of K from Eq. (23). Further, the self-energy is

$$\Sigma(\omega) = -b_0 = \frac{i}{2}\sqrt{2-(\omega+\mu)^2} - \frac{1}{2}(\omega+\mu) \qquad (28)$$

and has a nonzero imaginary part at the Fermi surface ($\omega=0$), corresponding physically to scattering by spin disorder. However, this scattering is not too strong. From Eqs. (28) and (11) one finds that the product of the imaginary part of the self-energy and the density of states at the Fermi level is $(2-\mu^2)/\pi$. This number is rather less 1, and implies a mean free path longer than p_F^{-1}. This spin disorder scattering decreases as T is decreased below T_c.

The model with $\lambda=0$ was studied in the dynamical mean-field method by Furukawa,[15] who obtained Eq. (28). Furukawa also used a method he referred to as solving the equations at constant magnetization to produce an interpolation formula describing the temperature dependence of Σ'' for $0 \leq T \leq T_c$. We believe these results are similar but not quite equivalent to those we obtain by solving Eqs. (16) directly. However, the minor differences between Furukawa's results and ours are not important. The main point is that the scattering at $T>T_c$ predicted by this calculation is much too small to explain the data.

One may calculate T_c at zero coupling by linearizing the second of Eqs. (16) in b_1. One finds that $T_c(\mu)$ is given by the solution of

$$T_c(\mu) = -\int_{-\sqrt{2}}^{\sqrt{2}} \frac{d\omega}{\pi} f((\omega-\mu)/T_c(\mu)) \frac{\omega\sqrt{2-\omega^2}}{8/3-\omega^2}, \quad (29)$$

where f is the Fermi function.

We now return to the issue of the effects of the electron-phonon coupling. At $T=0$ the mean-field equation is identical to that considered in I. From this work we learn that there are three regimes: *weak coupling*, in which $\lim_{T\to 0}\bar{x}^2(T)=0$, $\lim_{T\to 0}\rho(T)=0$, and $d\rho/dT|_{T=0}\sim\lambda$; *intermediate coupling*, where $0<\lim_{T\to 0}\bar{x}^2(T)<\bar{x}_c^2\sim 1$, $0<\lim_{T\to 0}\rho(T)<\infty$, and $d\rho/dT|_{T=0}$ may have either sign, and *strong coupling*, where $\bar{x}_c^2<\lim_{T\to 0}\bar{x}^2(T)$ and $\lim_{T\to 0}\rho(T)=\infty$. Here x_c is the value of frozen-in lattice distortion above which a gap appears in the electron spectral function. In the strong coupling regime one may think of the electrons as being localized as polarons.

Another crucial result of I is that the transitions between the different regimes are controlled by the values of an effective coupling determined by the ratio of an electron-phonon energy to a kinetic energy. As we have seen, the kinetic energy is temperature dependent because of double exchange; thus as temperature is varied the behavior of the model may change from ''metallic'' ($d\rho/dT>0$) to insulating ($d\rho/dT<0$). As T is decreased below T_c there are two effects causing a decrease in the resistivity: the spin scattering freezes out and the effective electron-phonon coupling weakens.

IV. HALF FILLING

In the section we present and discuss results of numerical calculations for the particle-hole symmetric ($n=1$) case. We begin with ferromagnetic T_c shown in Fig. 2. One sees that T_c decreases with increasing λ; the variation is particularly rapid in the region $\lambda\approx 1$, which is shown below to be the critical value at which the model goes from metal to insulator.

For $n=1$ and all λ we verified that the transitions were second order by comparing the T_c obtained in this manner to the T_c obtained by determing the temperature at which the nonmagnetic state becomes linearly unstable. We also checked for metastability at various n and λ by starting our iterations with saturated magnetization $[b_1=b_0-(\omega+\mu)]$ and with very small b_1, and verifying that both initial conditions converged to the same solution. The magnetic transition was always found to be second order.

It is interesting to compare our results to those of Ref. 23. The method used by these authors to treat the magnetic fluctuations is very similar to the ''projection method'' discussed at the end of Sec. II. We found that the method did not give an accurate value for T_c but did reproduce the coupling dependence well. Reference 23 used a model with one orbital per site; we should therefore compare their results for $n=1/2$ to ours for $n=1$. Their quantity $\epsilon_p=\lambda_{JT}^2/2K$ corresponds precisely to our λ; the factor of 2 comes from the orbital degeneracy as explained in our companion paper I. As far as can be determined from Fig. 1 of Ref. 23, their calculated $T_c(\epsilon_p)/T_c(0)$ agrees very well with our $T_c(\lambda)/T_c(0)$. The correspondence is interesting because the calculation of Ref. 23 was done with quantum phonons with the rather high frequency $\omega=0.5$ (units not specified, but presumably set by the electron hopping t). This supports our claim that quantum effects are not important at temperatures of the order of T_c. We believe that caution is required in interpreting the results presented in Ref. 23 for the doping dependence of T_c because this work is based on a model with one orbital per site, which therefore has no kinetic energy at $n=1$. The authors argue that the one-orbital model is justified by the existence of the Jahn-Teller splitting. Our results show that this is not the case. We discuss the physics of the doping dependence of T_c further in the Conclusion.

We now turn to the temperature dependence of the resistivity, shown in Fig. 3. The curves display kinks at the ferromagnetic T_c. The resistivity drops as T is decreased below T_c both because the magnetic contribution to the scattering begins to decrease at T_c and because the effective electron-phonon interaction becomes weaker. From these curves we may distinguish ''metallic'' ($d\rho/dT>0$) and ''insulating'' ($d\rho/dT<0$) regimes. At $T>T_c$ $\lambda=1$ marks the boundary between metallic and insulating regimes; at $\lambda=1$, $d\rho/dT=0$. For $T<T_c$ the crossover occurs at the somewhat larger $\lambda\sim 1.15$. The difference in the critical λ required to produce insulating behavior reflects the effect of spin alignment on the electron kinetic energy. We also note that although it is difficult to perceive on the logarithmic scale used in Fig. 3, for $1.08<\lambda<1.15$, $\lim_{T\to 0}\rho(T)=\rho_0$ is neither zero nor infinite. For λ sufficiently close to 1.15, $\lim_{T\to 0}d\rho/dT<0$. Similar behavior was discussed at length in I.
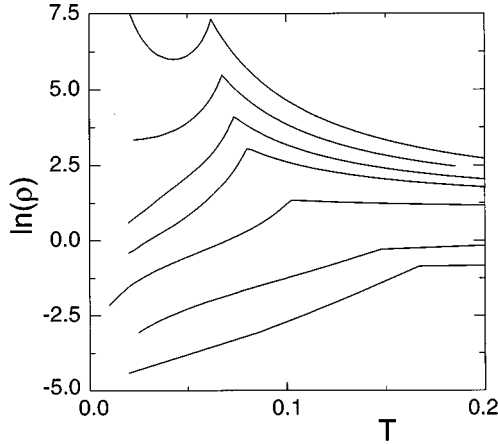
FIG. 3. Temperature dependence of resistivity at $n=1$ for couplings $\lambda=0.32$ (lowest curve), 0.71, 1, 1.08, 1.12, 1.15, and 1.20 (highest curve).

Figure 4 shows the temperature dependence of the mean square lattice distortion $\bar{x}^2$. From this one may distinguish the low-T *weak, intermediate*, and *strong coupling* regimes, based on the $T\to 0$ limit of $r(T)$. The regimes were discussed at length in I. Roughly, in *weak coupling* $r(T=0)=0$, in *intermediate coupling* $0<r(T=0)<1$, and in *strong coupling* $r(T=0)>1$. In intermediate coupling there is a frozen-in lattice distortion that affects the $T=0$ physics but is not large enough to open a gap; for strong coupling the distortion is large enough to open a gap and cause insulating behavior. For $r^2>0.25$, $\lim_{T\to 0} d\rho/dT<0$ even though if $r^2<1$, $\lim_{T\to 0}\rho(T)$ is finite.

The effects of double exchange may be seen in Fig. 4. T_c is visible as a kink on each curve. At $T>T_c$, dr^2/dT decreases, implying a stronger electron-phonon coupling. For $\lambda>0.9$ the $T=0$ values obtained by extrapolating the $T>T_c$ curves to 0 are nonzero, and are higher than the actual $T=0$ values, because the reduction of kinetic energy due to spin disorder has effectively made the electron-phonon coupling stronger. Note that the $T=0$ extrapolation of the $T>T_c$ portion of the curve corresponding to $\lambda=1.05$ is about $r^2=0.95$. This is slightly less than the critical value $r_c^2=1$ found in I to mark the boundary between finite and
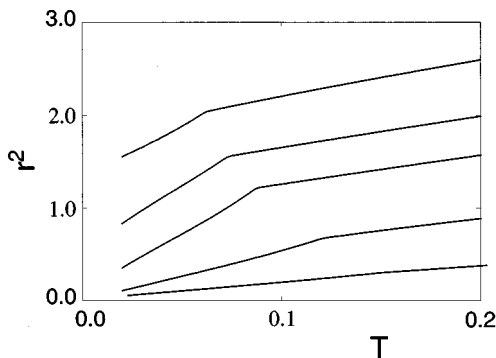

FIG. 4. Temperature dependence of mean square lattice distortion for $n=1$ and couplings $\lambda=0.71$ (lowest), 0.9, 1.05, 1.12, and 1.2 (highest).
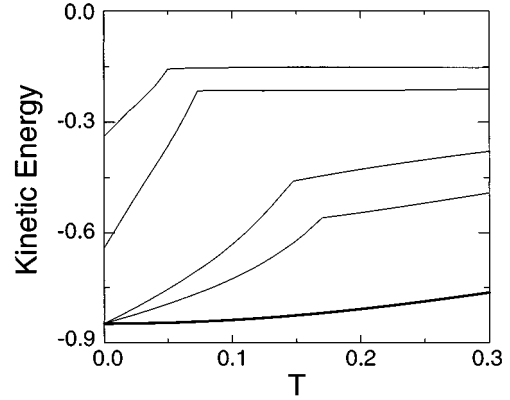

FIG. 5. Temperature (T) dependence of electron kinetic energy (K) for $n=1$ and $\lambda=0$ (second lowest curve), 0.71, 1.12, and 1.29 (highest curve). The lowest curve corresponds to $\lambda=0$ in the model without double exchange.

infinite $\rho(T=0)$ at $n=1$. From this we would infer at $T>T_c$, $d\rho/dT$ changes sign at $\lambda\gtrsim 1.05$, as indeed is seen in Fig. 3.

The curves presented in Fig. 4 show r^2 in arbitrary units. To estimate the magnitude of the effect in $Re_{1-x}A_xMnO_3$ we note that in $LaMnO_3$ each O ion is displaced ≈ 0.15 Å from its ideal perovskite position.[7] The estimates obtained in Ref. 20 imply $\lambda\approx 1.3-1.5$ in that material; thus $r^2=3$ in Fig. 4 corresponds to a rms displacement of an O ion of about 0.15 Å.

We next consider the temperature dependence of the kinetic energy shown in Fig. 5. At $\lambda=0$ the kinetic energy changes by about $1/\sqrt{2}=30\%$ between $T=0$ and $T=T_c$, and has a weak T dependence at $T>T_c$. For $\lambda=0.71$ the kinetic energy changes between 0 and T_c by a somewhat larger amount; for $\lambda=1.11$, by a still larger amount, for $\lambda=1.29$, yet larger. These changes come from the previously discussed interplay between double exchange and electron-phonon coupling. As T is increased from zero, the spins disorder. This reduces the electron kinetic energy and permits the electron-phonon coupling to further localize the electrons, reducing their coupling yet more, etc. We also note that we found the ratio between T_c and the kinetic energy at T_c to be the same within a few percent for all n and λ studied. For $n=1$ this can be seen by comparing Figs. 2 and 5.

These arguments also explain the magnetic field dependence of the resistivity. Increasing the field aligns the spins, increases the kinetic energy, and decreases the effective electron-phonon coupling, leading to a large change in resistance as shown in Figs. 6(a) and 6(b). When the decrease in effective electron-phonon coupling tunes the model across the "metal"-"insulator" transition, as in Fig. 6(b), the magnetoresistance is particularly large.

Further insight into the interplay of double exchange and localization comes from the optical conductivity shown in Fig. 7. Panel 7(a) shows $\sigma(\omega)$ at different T for the weak coupling $\lambda=0.7$. At low T σ has approximately the Drude form $\sigma(\omega)=\Gamma/(\omega^2+\Gamma^2)$ with scattering rate $\Gamma\sim T$ as expected from classical phonons. As T is increased through T_c the Drude peak broadens and acquires a T-independent
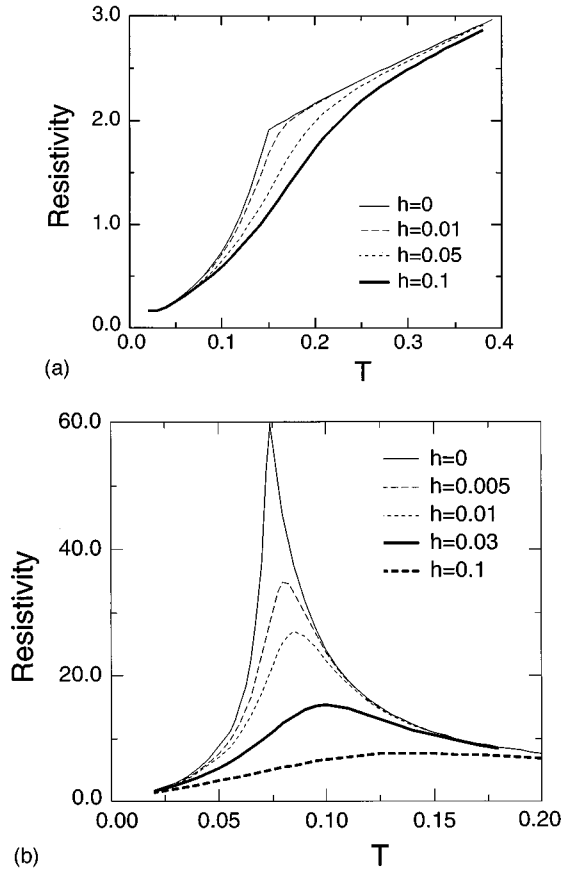
FIG. 6. Temperature dependence of resistivity at different values of magnetic field h for $\lambda = 0.7$ (a) and $\lambda = 1.12$ (b). The parameter h is related to the physical field h_{phys} by $h = g\mu_B S_c h_{phys}/t$. Using $g = 2$, $t = 0.6$ eV, and $S_c = 3/2$ means $h = 0.01$ corresponds to $h_{phys} = 15$ T.

FIG. 7. Optical conductivity, $n = 1$, $T = 0.02$ (light solid line), $T = T_c/2$ (light dashed line), $T = 3T_c/4$ (light dotted line), $T = T_c$ (heavy solid line), $T_c = 2T_c$ (heavy dashed line). (a) $\lambda = 0.71$ ($T_c = 0.15$), (b) $\lambda = 1$ ($T_c = 0.10$), (c) $\lambda = 1.08$ ($T_c = 0.08$), (d) $\lambda = 1.15$ ($T_c = 0.0675$). Note that in (a) the lowest T is 0.025 not 0.02, and $\sigma(\omega = 0)$ for this curve is 21.4.

part, due to spin scattering. Panel 7(b) shows σ for the moderate coupling $\lambda = 1$. At low T, σ has the Drude form; as T is increased a broad peak develops; this is due to transitions between the two Jahn-Teller split levels. It is broad because the phonon coordinate is strongly fluctuating, so the level position is not well defined. As T increases beyond T_c the peak broadens almost to indistinguishability. Note also that as T is increased, the optical spectral weight $\int d\omega \sigma(\omega)$ decreases, reflecting the increasing localization of electrons by phonons. In models such as the present one, which do not have Galilean invariance and involve only a limited number of orbitals, the f-sum rule spectral weight is not constant and is indeed proportional to the kinetic energy.[27] Panel 7(c) shows that at a stronger coupling σ does not have the Drude form, and the peak is already evident at $T_c/2$. Note that the maximum in σ has moved to a slightly higher frequency. Recently published data of Okimoto et al. on La$_{1.825}$Sr$_{.175}$MnO$_3$ (Ref. 8) are similar to the curves shown in Fig. 7(c), although our use of classical phonons means that we cannot obtain the very narrow Drude peak found at low T. Panel 7(d) shows σ at the still stronger coupling $\lambda = 1.15$ where the model has a large frozen-in lattice distortion even at $T = 0$. The σ has an insulating appearance, above and below T_c, but as T is decreased the peak in σ shifts to a lower freqency and grows in intensity, reflecting the effectively weaker coupling. The nonmonotonic behavior
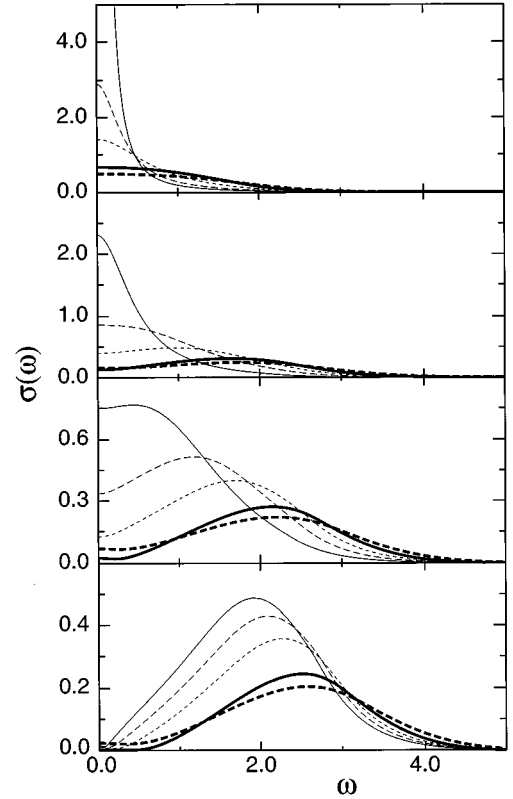
of the dc conductivity is not reflected in $\sigma(\omega)$ at $\omega \gtrsim 0.5$. The curves in Fig. 7(d) resemble data recently obtained by Kaplan et al. on Nd$_{0.7}$Ca$_{0.3}$MnO$_3$.[28]

We will discuss the physical interpretation of $\sigma(\omega, T)$ in more detail in the next section and in the Conclusion. Here we note that in the strong coupling regime the two d states on a site are split. The peak in the optical conductivity corresponds roughly to a transition in which an electron moves from an occupied orbital on one site to an unoccupied orbital on an adjacent site. In our classical approximation, "Franck-Condon" transitions involving also emission or absorption of a phonon cannot occur at all. In a more realistic model such effects would, e.g., increase the low-frequency tails by a small amount. The width of the peak in $\sigma(\omega)$ is determined by the broadening of the localized states due to electron hopping and by thermal broadening, which leads to a range of lattice distortions and thus to a range of splittings.

V. DIFFERENT DOPINGS

In this section we present and discuss results of numerical calculations for the particle-hole asymmetric case $n \neq 1$. As discussed in I (see especially Figs. 10, 11), at $n \neq 1$ in the strong coupling limit the spectral function has a three-peaked structure. The outer two peaks represent the Jahn-Teller-split e_g levels on occupied sites, and occur also for $n = 1$. The
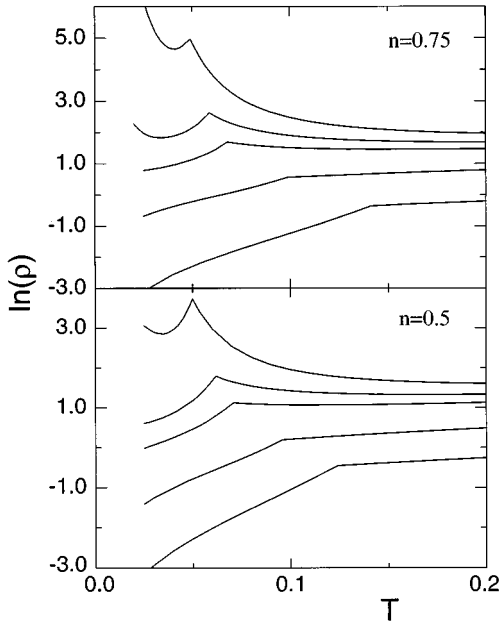
FIG. 8. Resistivity (ρ) vs temperture (T) for $n=0.75$ (upper panel) and $n=0.5$ (lower panel) and couplings $\lambda=0.71$ (lowest), 1.12, 1.41, 1.49, and 1.58 (highest).
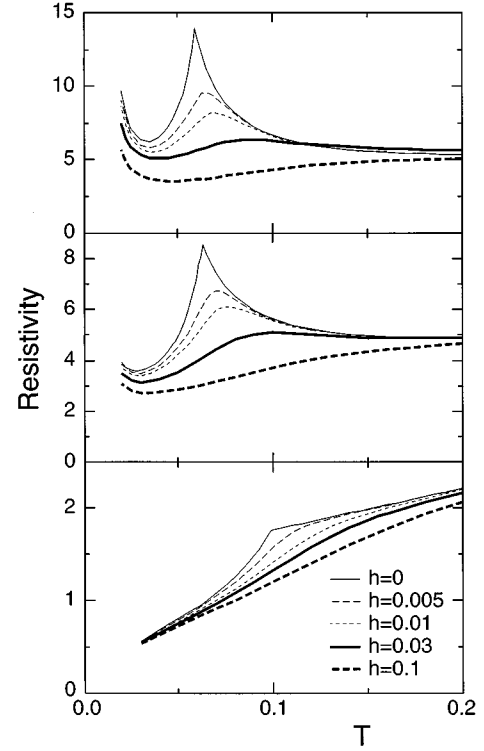

FIG. 9. Magnetic field dependence of resistivity for $n=0.75$ and $\lambda=1.12$ (lower panel), $\lambda=1.46$ (middle panel), and $\lambda=1.49$ (upper panel).

middle peak comes from unoccupied sites, on which there is no Jahn-Teller splitting. These states tend to fill in the gap created by the Jahn-Teller splitting and mean that stronger coupling is required to obtain insulating behavior at $n\neq1$ than at $n=1$. Further, in the strong coupling limit the temperature dependence of physical quantities is determined by the energy difference between filled and midgap states; thus at fixed Jahn-Teller splitting the activation gap for physical properties is much less at $n\neq1$ than at $n=1$. Note also that T_c is controlled by the electron kinetic energy, which is in turn controlled by the Jahn-Teller splitting. Therefore, in the strong coupling limit at fixed T_c the activation gap characterizing the $T>T_c$ resistivity is much larger at $n=1$ than at $n\neq1$.

This physics is immediately apparent in the resistivity curves for $n=0.75$ and $n=0.5$ shown in Fig. 8. Comparison to Fig. 3 shows that much stronger couplings are required to obtain a $d\rho/dT<0$ for $n=0.75$ than for $n=1$ and stronger couplings yet are required for $n=0.5$. The smaller value of the activation gap relative to T_c means that the resistivity rises less before the behavior changes at T_c for $n\neq1$ than for $n=1$. For $n=1$, $\lambda=1.1$ we found an order-of-magnitude rise in ρ as T is decreased to T_c, and we found metallic behavior below T_c. At $n\neq1$ it is difficult to produce much of an up-turn in ρ at $T>T_c$ for parameters such that the model is metallic at $T=0$. This physics is due to the particular (Jahn-Teller) form of the electron-phonon coupling we have chosen to study.

The same arguments mean that it is not possible to get as large a magnetoresistance at $n\neq1$ as at $n=1$. Figure 9 shows the temperature dependence of the resistance for several different coupling strengths and magnetic fields. To get even a moderately large effect one must choose a very strong coupling, such that the model is insulating for both $T>T_c$ and $T<T_c$.

Finally, Fig. 10 displays the temperature dependence of the optical conductivity at $n=0.75$ and moderate ($\lambda=1.29$) and strong ($\lambda=1.49$) coupling, and compares this to the momentum-integrated spectral functions. One sees by comparing energies that at strong coupling the two maxima in the conductivity may be associated with transitions from the lowest peak in the spectral function (representing occupied orbitals on occupied sites) to the middle feature (representing unoccupied orbitals on unoccupied sites) and to the higher feature (representing unoccupied orbitals on occupied sites). At $n=1$ the middle peak in A is absent and σ has only one peak, as seen in Fig. 7(d). Of course, the on-site d-d transition is not optically active: the calculated conductivity involves electron motion from one site to another, and for this reason σ is not simply given by a convolution of two local spectral functions. One may see this in Fig. 10. The central peak in $A(\omega)$ has less area than the upper one, yet the lower peak in the corresponding $\sigma(\omega)$ is the larger. This may be understood from the above arguments: a transition from the lower to the middle peak of $A(\omega)$ necessarily involves moving an electron from one site to the other, but some of the transitions from lower to higher are on-site transitions that do not contribute to σ.

Note also that the $T=2T_c$ spectral function shown in Figs. 10(b) and 10(d) has a sharp minimum at $\omega+\mu=0$. This is a consequence of the fact, discussed in I, that the probability of a small-amplitude lattice distortion is small because of the $x\,dx$ measure, and decreases as T increases, due to the shift to higher $\langle x^2\rangle$ of $P(x)$. As can be seen in the corresponding optical conductivity curves in Figs 10(a) and
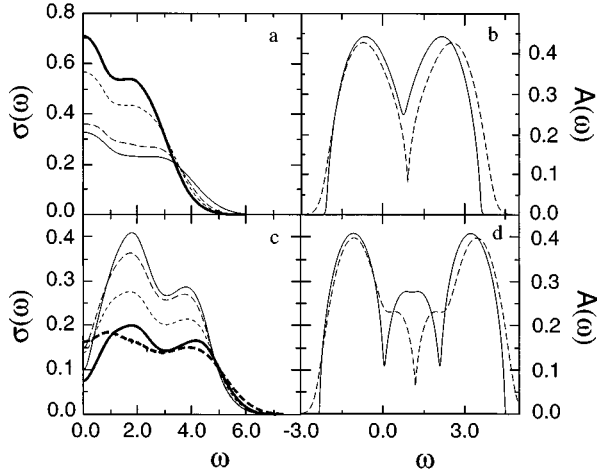
FIG. 10. Optical conductivities and spectral functions for $n=0.75$, $\lambda=1.29$ (a), (b) and $\lambda=1.49$ (c), (d). (a) $\sigma(\omega)$, $\lambda=1.29$, $T=0.04$ (light solid line), $T=0.061$ (light dashed line), $T=0.081=T_c$ (light dotted line), and $T=0.162$ (heavy solid line). (b) Spectral function, $\lambda=1.29$, $T=0.04$ (solid line), and $T=0.162$ (dashed line). (c) $\sigma(\omega)$, $\lambda=1.49$, $T=0.02$ (light solid line), $T=0.028$ (light dashed line), $T=0.045$ (light dotted line), and $T=0.059=T_c$ (heavy solid line) and $T=0.115$ (heavy dashed line). (d) Spectral function, $\lambda=1.49$, $T=0.02$ (solid line), and $T=0.115$ (dashed line).

10(c), this minimum is of little significance for other physical quantities.

VI. CONCLUSION

We have used the ''dynamical mean-field'' approximation to solve a model of electrons ferromagnetically coupled to classical spins and Jahn-Teller coupled to localized classical oscillators. In a companion paper (I) we considered electron-phonon coupling in a variety of models without double exchange. The results presented in Sec. IV for the half-filled case bear a striking resemblance to data for the ''colossal magnetoresistance'' materials $Re_{1-x}A_xMnO_3$ in the $0.2 < x < 0.5$ regime where the ground state is metallic. We believe the agreement supports the idea that the important physics of $Re_{1-x}A_xMnO_3$ involves the interplay between a strong electron-phonon coupling and the ''double exchange'' effect of magnetic order on the electronic kinetic energy. Specifically, the $\rho(T)$ curves shown in Fig. 3 are very similar to those shown, e.g., in Refs. 29 and 30. Varying the electron-phonon coupling produces changes very similar to those found experimentally by varying x and the constituents Re and A. The magnetic field dependences shown in Fig. 6 also bear a striking resemblance to data. Figure 6(b) looks very much like Fig. 2 of Ref. 33, while Fig. 6(a) resembles magnetoresistance data that would be observed for $La_{1.6}Sr_{0.4}MnO_3$. (It should be noted, however, that the fields used to produce our curve, although very small compared to microscopic energies, are larger than experimental fields by a factor of about 5.) The variation of the rms lattice distortion shown in Fig. 4 has been observed via measurements of the e_g component of the oxygen Debye-Waller factor.[31,32]

Further, optical conductivity data of Okimoto *et al.*[8] on $La_{1.825}Sr_{.175}MnO_3$ bear a strong qualitative resemblance to Fig. 7(c), while data obtained by Kaplan *et al.*[28] strongly resemble Fig. 7(d). As noted in Secs. IV and V, in our interpretation the higher-frequency peak in $\sigma(\omega)$ is due to transitions between levels split by an electron-phonon coupling. Okimoto *et al.* interpreted the higher peak differently, attributing it to transitions from an inital e_g state aligned to the core spin to a final e_g state antialigned to the core spin. They argued that their identification was supported by the fact that in their data the higher peak was only visible at $T > T_c$, and vanished at low T when all spins were aligned. However, the data of Kaplan *et al.* demonstrate that in some samples the high-frequency peak does not vanish below T_c and indeed grows in oscillator strength as T decreases. This rules out the interpretation of Okimoto *et al.*, at least for samples such as those studied in Ref. 28.

The detailed qualitative agreement between data and our model leaves little doubt that we have identified the important physics governing the $Re_{1-x}A_xMnO_3$ materials. However, several very important issues remain unresolved. One concerns the origin of the experimentally observed material and doping dependence of the results, which are *modeled* in the $n=1$ calculations by varying the electron-phonon coupling. Another is the degree of ''fine-tuning'' of parameters required. A third concerns the effects of omitted interactions and a fourth is that, as shown in Sec. V, computations at different electron concentrations $n \neq 1$ agree much less well with data. In the remainder of this paper we present a qualitative discussion of all of these issues, which, we argue, are closely related.

We begin with the $n \neq 1$ calculations. We showed that the differences between the $n=1$ and $n=0.75,0.5$ results are due to the presence, for $n \neq 1$, of midgap states in the spectral function (shown, e.g., in Fig. 10). These midgap states occur because we used a particular form of electron-phonon coupling, namely, a Jahn-Teller coupling that splits the d-state degeneracy on a site if there is one electron on the site, and does nothing otherwise. In Ref. 23 it is argued that the existence of the Jahn-Teller coupling justifies a model involving only one orbital per site. The results presented here suggest that this is oversimplified, because it does not take into account the midgap states. A model with only Jahn-Teller coupling does not suffice. However, results presented in I and Ref. 23 strongly suggest that if the model were extended in a way that moved both the upper peak and the midgap states up in energy, then the model would become effectively a single-orbital model and results for $n \neq 1$ would much more closely resemble those obtained for $n=1$.

One omitted piece of physics that will have precisely this effect is the breathing-mode distortion of the oxygen octahedron around a Mn site. The breathing mode couples to charge fluctuations on the Mn site. This coupling is likely to be at least as strong as the Jahn-Teller coupling, as may be seen from the following argument: the Jahn-Teller coupling is due to the dependence of the force exerted on an O ion on the orbital occupied by the outer-shell d electron. Whatever its magnitude, this force is unlikely to be larger than the force created by simply removing that d electron, and making an unbalanced charge. The breathing-mode coupling was recently argued to be important for the small-x structural phase boundary.[20] To understand the effects of the breathing

mode, consider again Fig. 10. The central peak in the spectral function depicted in the low-T curve in Fig. 10(d) gives the states available for adding an electron to an unoccupied site. If such a site has a breathing distortion already present, the energy cost of adding an electron will be increased, thus the middle feature will also move up in energy, increasing the gap as required.

Another important piece of physics is the on-site Coulomb interaction. This must be strong because if it were not, the Hund's coupling J_H would not be large.[17] The Coulomb interaction leads to two related effects. One is most easily discussed by reference to the spectral functions and optical conductivities shown in Fig. 10. Now the $\omega > 0$ part of the spectral function corresponds to states into which an electron may be added; the upper peak thus gives the states available for adding an electron onto a site that already has an electron. The Coulomb interaction must move such states up in energy, and must similarly move up the second peak in $\sigma(\omega)$. If the Coulomb energy is of the order of the Hunds coupling, then it is very likely that this effect will move the higher peak out beyond the physically interesting energy range $\omega \lesssim 3$ eV.

The combined effect of the breathing distortion and the Coulomb interaction is therefore to lead to a spectral function with at most two peaks in the energy range of interest. The only difference between this realistic situation and the situation encountered in the $n=1$ calculations is that the realistic spectral function is not symmetric under the interchange of the two peaks. This asymmetry was shown in I not to be important.

A second effect of a strong Coulomb interaction is to localize the electrons. It is likely that the observed very strongly insulating behavior of ReMnO$_3$ is not due solely to the Jahn-Teller order, and that ReMnO$_3$ is to some degree a Mott insulator. Now the kinetic energy K of a Mott insulator has a pronounced doping dependence.[27] For $Re_{1-x}A_xMnO_3$ one would expect $K(x)$ to increase with x for $x<0.5$. Because, as we have argued at length, the properties of electron-phonon models are controlled by the ratio of a coupling energy and a kinetic energy, this will lead to an x dependence of the effective coupling strength, with larger x having a weaker effective coupling. We believe that this strong x dependence of the effective coupling accounts for the ubiquity of the "colossal" magnetoresistance phenomenon. Different materials have different bare electron hoppings and probably different electron-phonon couplings, but in all materials the variation of the electron kinetic energy with x is large enough to sweep the effective coupling through the critical value at some x between 0.1 and 0.5.

The breathing distortion may be studied via the dynamical mean-field formalism used here; one must simply integrate over another variable in Eq. (12). The on-site Coulomb interaction may also be included, but one must perform functional integrals rather than simple integrals. Monte Carlo techniques are required, the computational expense is greater, and the accuracy is less. Such an investigation would, however, be desirable.

Two other effects not included in the calculation should be mentioned. Quantum fluctuations of the phonons have been omitted. As discussed in I, these will in the absence of long-range order or commensurate density lead to metallic behavior at sufficiently low T, even in the strong coupling limit. The neglect of the phonon momentum and quantum fluctuations of core spins is not an important approximation because we are primarily interested in phenomena at temperatures of order room temperature; however, if needed they could be incorporated into the formalism. The neglect of intersite phonon correlations is potentially more serious. It is tempting to argue that they are unimportant because we are interested in optical phonons, which are usually weakly dispersing. However, in the ReMnO$_3$ structure each O is shared by two Mn; there must thus be a strong correlation between Jahn-Teller distortions on adjacent sites. In LaMnO$_3$ the Jahn-Teller distortions have long range order; estimates presented in Ref. 20 suggest that in $Re_{1-x}A_xMnO_3$ the correlation length of the Jahn-Teller distortions is $\sim x^{-1}$ as long as the resistivity is well above the Mott limit. Extending the present calculations to include the effects of intersite correlations is an important open problem. It is worth addressing because in the present calculations the correlation length is zero and the strong-coupling physics is of polarons. In the infinite correlation length limit, the physics has to do with interband transitions in a band structure defined by Jahn-Teller order. The situation in the actual materials is presumably intermediate between these two limits.

Note added.—Very recently, a paper by Zang, Bishop, and Roder has appeared, which presents a somewhat different view of the physics considered here.[34] In this work long-ranged Jahn-Teller order was assumed to occur at low T, and the combined effect of orientational fluctuations of the Jahn-Teller distortion and double exchange on the resistivity was studied.

APPENDIX A: ANALYSIS OF OBSERVED RESISTIVITY

In this Appendix we discuss the observed $T>T_c$ resistivities of $Re_{1-x}A_xMnO_3$. We note that the observed strong x dependence suggests that the number of active carriers is x. For x classical particles hopping with *probability* W on a cubic lattice of lattice constant a,

$$\sigma = \frac{e^2 x W}{3 a k_B T}. \tag{A1}$$

Using $a \approx 4$ Å as appropriate to $Re_{1-x}A_xMnO_3$ we have

$$\frac{\hbar W}{k_B T} = \frac{5 \times 10^{-4}}{x \rho(\Omega\text{-cm})}. \tag{A2}$$

From this equation one may easily see that observed resistivities, which are typically greater than 0.01 Ω cm at $T > T_c$ and $x \lesssim 0.3$, and increase rapidly with decreasing x imply values of $\hbar W / k_B T$ much less then unity. If $\hbar W / k_B T \ll 1$, a particle has time to thermalize before it moves, and a classical model is appropriate.

APPENDIX B: RESISTIVITY OF DOUBLE-EXCHANGE-ONLY MODEL

In this Appendix we consider in more detail the resistivity of the double-exchange-only model. In this model, resistivity comes from spin disorder. It is maximal at $T \gg T_c$ and vanishes at $T = 0$. The resistivity has been calculated, using methods that are essentially perturbative in the amplitude of the spin disorder, by Kubo and Ohata[14] and more recently by two of us and Littlewood.[16] The spin scattering was found not to be too strong. As discussed in the text, similar results have been obtained using the dynamical mean-field method by us and by Furukawa.[15] Because these calculations omit several physical effects they have been questioned recently by Varma.[17] In this Appendix we show that the omitted effects are not important.

We begin by describing the omitted effects. In the double-exchange-only model, the scattering is due to spin disorder, which, if the core spins are assumed to be classical, may be treated as static scattering with the important proviso that the disorder is annealed, not quenched. When applied to a model with static scattering, the dynamical mean-field approximation with semicircular density of states is equivalent to the coherent potential approximation (CPA) for the Bethe lattice.[21] The CPA neglects localization (as do the perturbative calculations.[14,16]) The lack of closed loops on the Bethe lattice also means that Berry phase effects arising from particle motion in a spin background are omitted.

We consider the Berry phase effects first. In the double exchange model the hopping matrix element between two sites i and j is with core spins characterized by polar angles (θ_i, ϕ_i), (θ_j, ϕ_j), is

$$t_{ij} = t \left(\cos\frac{\theta_i}{2}\cos\frac{\theta_j}{2} + \sin\frac{\theta_i}{2}\sin\frac{\theta_j}{2} e^{i(\phi_i - \phi_j)} \right). \quad \text{(B1)}$$

If closed loops are not important one may choose the ϕ_i independently on each site and recover the familiar double exchange result $t_{ij} = t\cos(\theta_i - \theta_j)/2$. In general the ϕ factors around a closed loop produce something like a magnetic field, which may scatter electrons. In the limit of strong ferromagnetic correlations the phase-dependent term may be seen to be very small because all nearby sites have very similar angles, which may be taken to be near 0. In the limit

of uncorrelated spins we may estimate the size of the effective field by comparing the phase sensitive part of the hopping to the phase insensitive $\cos(\phi_i - \phi_j)/2$ part. By integrating t_{ij}, around square placquette one finds that the phase sensitive part is $(t^4/16)e^{2i\phi_i}$ while the phase insensitive part is $t^4/4$. Thus the rms deviation of the amplitude for an electron to move around a plaquette is $1/4\sqrt{2}$ of the phase insensitive part. This, combined with the relative insensitivity of three-dimensional physics to closed loops, suggests that phase effects, while interesting, are too weak to cause the observed strongly insulating behavior.

We now turn to localization. The problem at hand concerns electrons with random hopping, which has not received much attention. Economou and Antoniou[35] have studied a Bethe-lattice model in which the hopping amplitude t has the symmetrical distribution

$$P_E(t) = \frac{2}{\pi t_1} \sqrt{t_1^2 - (t - t_0)^2}. \quad \text{(B2)}$$

For this model $\bar{t}$, the mean value of t, equals t_0 and the variance $\langle (t - \bar{t})^2 \rangle = t_1^2/4$. The double exchange model at $T \gg T_c$ (so the spins are completely disordered) corresponds to the distribution

$$P_{d\text{-ex}}(t) = \frac{2t}{t_D^2}\theta(t_D - t). \quad \text{(B3)}$$

The localization effects of the double exchange distribution have not been determined. We expect that because the most probable value is also the largest hopping, the double exchange distribution will produce fewer localized states than a semicircular distribution with the same mean and variance. Now from Eq. (B3) one sees that the double exchange distribution has mean $\bar{t} = 2t_D/3$ and variance of $t_D^2/18$. Thus it should produce fewer localized states than the model of Economou and Antoniou with $t_0 = 2t_D/3$ and $t_1 = \sqrt{2}t_D/3$, i.e., with $t_1/t_0 = 1/\sqrt{2}$. Inspection of Ref. 35 reveals that at this ratio of t_1/t_0, a negligible fraction of the states are localized. We therefore conclude that localization effects are not important. Reference 17 on the contrary asserts that the double exchange model with completely disordered spins is better modeled by the Economou-Antoniou distribution with t_1/t_0 somewhat larger than unity, so a non-negligible fraction of the states are localized. Drawing precise conclusions is somewhat difficult because one result of Ref. 35 is that the number of localized states increases rapidly for $t_1/t_0 > 1$. Nevertheless, we believe the estimate $t_1/t_0 \approx 0.7$ obtained above shows that localization effects are unlikley to be important.

[1] E. D. Wollan and W. C. Koehler, Phys. Rev. **100**, 545 (1955)

[2] J. Goodenough, Phys. Rev. **100**, 564 (1955).

[3] S. Jin, T. H. Tiefel, M. McCormack, R. A. Fastnacht, R. Ramesh, and L. H. Chen, Science **264**, 413 (1994).

[4] G. F. Koster, A. Dimmock, R. G. Wheeler, and H. Statz, *Representations of the 32 Point Groups* (MIT Press, Cambridge, MA, 1963).

[5] L. F. Mattheiss (unpublished).

[6] J. Kanamori, J. Appl. Phys. Suppl. **31**, 14S (1961).

[7] J. B. A. A. Ellemans, B. vanLaar, K. J. R. vanderVeer, and B. O. Loopstra, J. Solid State Chem **3**, 238 (1971).

[8] Y. Okimoto, T. Katsufuji, T. Ishikawa, A. Urushibara, T. Arima, and Y. Tokura, Phys. Rev. Lett **75**, 109 (1995).

[9] See, e.g., N. F. Mott, in *Disordered Semiconductors*, edited by M.

A. Kastner, G. A. Thomas, and S. R. Ovshinsky (Plenum, New York, 1987), p. 3.

[10] C. T. Chen, Y. Tomioha, A. Asamitsu, H. Kuwahara, Y. Moritomo, and Y. Tobura, Phys. Rev. B **53**, 1698 (1993); A. P. Ramirez, P. Schiffer, S.-W. Cheong, C. H. Chen, W. Bao, T. T. M. Palstra, P. L. Gammel, D. J. Bishop, and B. Zegarski, Phys. Rev. Lett. **76**, 3188 (1996).

[11] P. W. Anderson and H. Hasegawa, Phys. Rev. **100**, 675 (1955).

[12] P. G. deGennes, Phys. Rev. **118**, 141 (1960).

[13] R. Searle and C. Wang, J. Phys. **48**, 2023 (1970).

[14] K. Kubo and A. Ohata, J. Phys. Soc. Jpn. **33**, 21 (1972).

[15] N. Furukawa, J. Phys. Soc. Jpn. **63**, 3214 (1994).

[16] A. J. Millis, P. B. Littlewood, and B. I. Shraiman, Phys. Rev. Lett. **74**, 5144 (1995).

[17] C. M. Varma, Phys. Rev. B (to be published).

[18] For an example of the resistivity of $La_{2-x}Sr_xCuO_4$ see, e.g., H. Y. Hwang *et al.*, Phys. Rev. Lett. **72**, 2636 1994.

[19] For examples of resistivities of electronically three-dimensional transition metal oxides see, e.g., Y. Tokura, Y. Taguchi, Y. Okada, Y. Fujishima, T. Arima, K. Kumagai, and Y. Iye, Phys. Rev. Lett. **70**, 2126 (1993).

[20] A. J. Millis, Phys. Rev. B **53**, 8434 (1996).

[21] For a review, see A. Georges *et al.*, Rev. Mod. Phys. **68**, 13 (1996).

[22] D. Emin, M. Hillery, and N-L. H. Liu, Phys. Rev. B **33**, 2933 (1986).

[23] H. Roder, J. Zang, and A. R. Bishop, Phys. Rev. Lett. **76**, 1356 (1996).

[24] A. J. Millis, B. I. Shraiman, and R. Mueller, Phys. Rev. Lett. (to be published).

[25] A. J. Millis, R. Mueller, and B. I. Shraiman, preceding paper, Phys. Rev. B **54**, 5389 (1996).

[26] A. Abrikosov, L. P. Gorkov, and I. E. Dzyaloshnski, *Methods of Quantum Field Theory in Statistical Physics* (Dover, New York, 1993).

[27] See, e.g., A. J. Millis and S. N. Coppersmith, Phys. Rev. B **42**, 10 807 (1990).

[28] S. G. Kaplan, U. M. Quijade, H. D. Drew, G. C. Xiong, R. Ramesh, C. Meuon, T. Venkatesan, and D. B. Tanner (unpublished).

[29] Y. Tokura, A. Urushibara, Y. Moritomo, T. Arima, A. Asamitsu, G. Kido, and N. Furukawa, J. Phys. Soc. Jpn. **63**, 3931 (1994).

[30] H. Y. Hwang, S.-W. Cheong, P. G. Radaelli, M. Marezio, and B. Batlogg, Phys. Rev. Lett. **75**, 914 (1995).

[31] P. Dai, J Zhang, H. A. Mook, S-H. Liou, P. A. Dowben, and E. W. Plummer, Solid State Commun. (to be published).

[32] P.G. Radaelli, M. Marezio, H. Y. Hwang, S-W. Cheong, and B. Batlogg (unpublished).

[33] P. Schiffer, A. Ramirez, W. Bao, and S-W. Cheong, Phys. Rev. Lett. **75**, 3336 (1995).

[34] J. Zang, A.R. Bishop and H. Roder, Phys. Rev. B **53**, 8840 (1996).

[35] E. N. Economou and P. D. Antoniou, Solid State Commun. **21**, 285 (1977).